Science of the Total Environment 831 (2022) 154857

Contents lists available at ScienceDirect

Science of the Total Environment

journal homepage: www.elsevier.com/locate/scitotenv

Development of magnetic nanoparticle assisted aptamer-quantum dot based biosensor for the detection of *Escherichia coli* in water samples

Chitvan Pandit [a,1], Hema Kumari Alajangi [a,b,1], Joga Singh [a,1], Akhil Khajuria [a,1], Akanksha Sharma [a,b], Md. Samim Hassan [c], Manmohan Parida [d], Anil Dutt Semwal [d], Natarajan Gopalan [e], Rakesh Kumar Sharma [f], Ashish Suttee [g], Udit Soni [h], Bhupinder Singh [a], Sameer Sapra [c], Ravi Pratap Barnwal [b,*], Gurpal Singh [a,*], Indu Pal Kaur [a,*]

[a] University Institute of Pharmaceutical Sciences, Panjab University, Chandigarh, India
[b] Department of Biophysics, Panjab University, Chandigarh, India
[c] Department of Chemistry, Indian Institute of Technology Delhi, New Delhi, India
[d] Defence Food Research Laboratory, Mysore, India
[e] Department of Epidemiology and Public Health, School of Life Sciences, Central University of Tamil Nadu, India
[f] Saveetha Institute of Medical and Technical Sciences, Tamil Nadu, India
[g] Department of Pharmacognosy, School of Pharmaceutical Sciences, Lovely Professional University, Phagwara, Punjab, India
[h] Department Department of Biotechnology, TERI School of Advanced Studies New Delhi, India

HIGHLIGHTS

- A biosensor for on-spot detection of *E. coli* in water samples using specific aptamer has been developed.
- Quantitative and qualitative ability for precise estimation of *E. coli*.
- Arduino 328P microcontroller used for cost effective and sensitive detection of the pathogen.
- The biosensor is capable of detection of lowest limit of 1×10^2 bacterial cells.
- This technology can be utilized for bacterial detection in various samples.

GRAPHICAL ABSTRACT

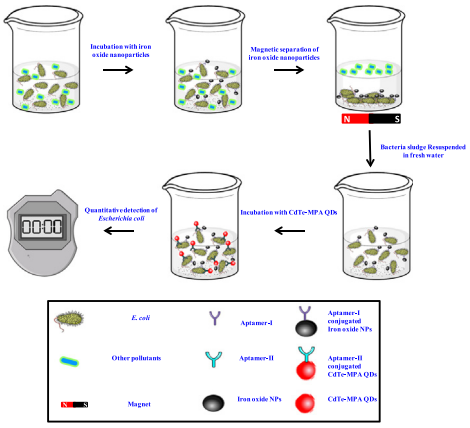

ARTICLE INFO

Editor: Warish Ahmed

Keywords:
E. coli
Portable biosensor
Aptamer
CdTe MPA QDs
SPIONs

ABSTRACT

The contamination of food and potable water with microorganisms may cause food-borne and water-borne diseases. The common contaminants include *Escherichia coli* (*E. coli*), *Salmonella* sp. etc. The conventional methods for monitoring the water quality for the presence of bacterial contaminants are time-consuming, expensive, and not suitable for rapid on-spot detection in field conditions. In the current study, super paramagnetic iron oxide nanoparticles (SPIONs) were synthesized and conjugated with *E. coli* specific Aptamer I to detect *E. coli* cells qualitatively as well as quantitatively. The sludge consisting of *E. coli*- SPION complex was separated via magnetic separation. The presence of *E. coli* cells was confirmed with the help of standard techniques and confocal laser scanning microscopy (CLSM) employing Aptamer II conjugated CdTe-MPA quantum dots (QDs). Finally, an ATmega 328P prototype biosensor based on

* Corresponding authors.
E-mail addresses: barnwal@pu.ac.in (R.P. Barnwal), gurpalsingh.ips@gmail.com (G. Singh), indupalkaur@yahoo.com (I.P. Kaur).
[1] Equal Contribution (Chitvan Pandit, Hema Kumari Alajangi, Joga Singh, Akhil Khajuria).

http://dx.doi.org/10.1016/j.scitotenv.2022.154857
Received 24 December 2021; Received in revised form 14 March 2022; Accepted 23 March 2022
Available online 26 March 2022

Aptamer II conjugated CdTe MPA QDs exhibited quantitative and qualitative abilities to detect *E.coli*. This prototype biosensor can even detect low bacterial counts (up to 1×10^2 cfu) with the help of a photodiode and plano-convex lens. Further, the prototype biosensor made up of ultraviolet light-emitting diode (UV LED), liquid crystal display (LCD) and ATmega328Pmicrocontroller offers on-spot detection of *E.coli* in water samples with high resolution and sensitivity. Similarly, this *in-house* developed prototype biosensor can also be utilized to detect bacterial contamination in food samples.

1. Introduction

Microorganisms are abundantly present in the soil, food, and water (Chandran and Mazumder, 2016). Lately, bacterial and viral diseases due to contamination of water bodies have become a global health concern. Water contaminated with pathogenic microorganisms acts as a source of origin and transmission of diseases. A Centers for Disease Control and Prevention (CDC) report documented that a whopping 60% of the global burden of diseases due to diarrheal illness is directly related to contaminated water (Investigating Outbreaks | Foodborne Outbreaks | Food Safety | CDC [WWW Document], n.d.). The primary causes of contamination of natural water reservoirs include urbanization, uncontrolled discharges from water recycling plants, hospitals, unchecked industrial effluents, sewage contamination, etc. (Chandran and Mazumder, 2016; Liu et al., 2012). According to an estimate, approximately 4.6% of disability-adjusted life years (DALYs) and 3.3% of deaths are attributed to water quality globally (Alahi and Mukhopadhyay, 2017).

Practically, a water sample cannot be tested for the presence of all the possible pathogens, so detection of common indicator organisms is carried out for assessing the water quality. As per the drinking water quality guidelines by the World Health Organization (WHO), 28 indicators organisms are categorized as water pathogens(WHO/UNICEF JMP, 2017). The list includes 12 bacteria, 8 viruses, 6 protozoa, and 2 parasites. The presence of indicator microorganisms is repeatedly considered as the pathogenic footprint of the water reservoir. Scientists have been testing water quality from lakes, rivers, and coastal bodies for human consumption by assessing the levels of *E. coli* and other coliforms in water samples (Borah et al., 2010; Sivasakthivel and Nandini, 2014). The group coliform includes various members of the family *Enterobacteriaceae*. These are commensals and normal inhabitants of the human intestinal tract. Among these, fecal coliform (or thermotolerant coliform) due to the abundant presence of *E. coli* is taken as an indicator of recent fecal contamination.

Various strains and serotypes of *E. coli* such as K-12, O157:H7 and CFT073 are pathogenic (Lukjancenko et al., 2010) and can cause urinary tract infections (UTIs), neonatal meningitis, gastroenteritis, etc. (Jang et al., 2017). Other pathogens present in water contaminated with the fecal matter may be more harmful and may cause a range of potentially fatal diseases like hepatitis A, typhoid fever, viral gastroenteritis etc. (Cabral, 2010; Gall et al., 2015). This is the major reason why *E. coli* is used as an indicator and its detection in water samples is crucial. Since surface water bodies are often used for recreational and drinking purposes, the presence of *E. coli* in waterways may increase the likelihood of human infection after exposure to these sources(Cho et al., 2018).

All the conventional methods used for the detection of *E. coli* are enumerative methods based on the fermentation of lactose. One of these is the most probable number (MPN) method used for the estimation of the total number of organisms in the sample. It consists of three steps (presumptive, confirmed and completed) for detection of *E. coli*, coliforms and fecal coliforms (or thermotolerant coliforms). A major drawback associated with the use of this test is that it is time-consuming, cannot be taken to the field for quick estimation, and requires skilled personnel. Further, a diagnostic technique like enzyme-linked immunosorbent assay (ELISA) has a high possibility of false-positive or negative results because of the insufficient blocking of the microtiter plate surface. Further, the process is time-consuming and requires skilled personnel for testing. Moreover, the tests cannot be taken at the sample site to assess sample's quality. Other sophisticated techniques like matrix-assisted laser desorption/ionization-time of flight (MALDI-TOF), polymerase chain reaction (PCR), and pulsed-field gel electrophoresis (PFGE) require huge initial capital, trained personnel, and lack instant detection capabilities. This calls for the development of simpler, faster, and on-the-spot detection techniques for pathogens like *E. coli*. In recent times, biosensors with biological selectivity and processing speed of the microelectronic circuit in combination with a bio-recognition system have revolutionized the area of microbial detection in water samples. These address almost all the pitfalls of conventional diagnostic tools. Biosensors have a distinctive edge in utilizing the whole range of biosensitive molecules viz.; oligonucleotides, antibodies and proteins for selectivity purposes. They have special applications in food safety and environmental research due to their high sensitivity for pathogenic contamination of the sample (Yi et al., 2020).

Biosensors capable of detecting *E. coli* in water would help in the quick resolution of water quality issues. A fluorescence-based biosensor has been developed for detecting *E. coli* based on the principle that 4-methylumbelliferyl-β-D-glucuronide (MUG) is rapidly hydrolyzed by an *E. coli* enzyme β-D-glucuronidase (GUD). It yields a fluorogenic product that is directly related to *E. coli* cells in water samples(Hesari et al., 2016). RNA Output Sensors Activated by Ligand Induction (ROSALIND) is a cell-free system for detecting various contaminants in water. This involves the use of an RNA aptamer which induces fluorescence. A contaminant stimulates the aptamer to transcribe and thus, leading to the production of fluorescent signals (Jung et al., 2020).

In the current study, we have developed *E. coli* aptamer I & II conjugated SPIONs and CdTe QDs ATmega328P prototype biosensor for both qualitative and quantitative detection of *E. coli* in water samples. A provisional Indian patent on the current work has also been successfully filed with the patent application number 202111024602.

2. Materials and methods

Escherichia coli (ATCC® 25922™) culture was procured from the Department of Biophysics, Panjab University, Chandigarh, India. Aptamers against *E. coli* were purchased from Eurofins Genomics India Pvt. Ltd. Goat anti-*E. coli* antibody was purchased from Bio-Rad Labs, India. Cadmium perchlorate hexahydrate, Iron (III) chloride hexahydrate (97%), 1-(3-Dimethylaminopropyl)-3- ethylcarbodiimide Hydrochloride), N-Hydroxysuccinimide, Oleic acids were purchased from TCI, Tokyo Japan. Rhodamine-6G, 1-Octadecene, 1, 2-Dichlorobenzene, 3-Mercaptopropionic acid, Zinc telluride, Tri-n-octylphosphine oxide, Tri-n-octylphosphine and *N*, *N*-dimethyl formamide were purchased from Sigma-Aldrich, USA. Luria Bertani medium, Agar, Potassium chloride, Sodium chloride, Sodium hydroxide, Ethanol, Hydrochloric acid, Acetone, Potassium hydrogen phosphate, Hexane, Citric acid (CA) and Diethyl ether were purchased from Sisco Research Laboratories Pvt. Ltd., India. ATmega 328P Development Board with Arduino was purchased from Macfos Pvt. Ltd., S5971 Photodiode, 70 pa, 900 nm, was purchased from Hamamatsu, Japan. Plano-convex lens was purchased from SD Optical Lab India. UV LED (395–400 nm) was purchased from Rhydo Technologies Pvt. Ltd., India.

2.1. Methods

2.1.1. Synthesis of nanoparticles

Ferric Oxide (Fe_3O_4) nanoparticles were synthesized by the thermal decomposition method as previously described (Jana et al., 2004) and Cadmium telluride-mercaptopropionic acid quantum dots (CdTe MPA QDs) were synthesized using direct aqueous method(Mittal and Sapra, 2015).

Detailed methodology of synthesis of the nanoparticles (NPs) is given in **Supplementary Information (SI)**.

2.2. Characterization of CdTe-MPA QDs and SPIONS

2.2.1. Particle size analysis

The mean diameter of the hydrophilic CdTe-MPA QDs and hydrophilic SPIONs ($n = 6$ batches prepared separately) was determined after appropriate dilutions (10 times) with double distilled water using Delsa™ Nano C Particle Analyser (Beckman Coulter, USA).

2.2.2. Polydispersity index (PDI)

The PDI of the synthesized hydrophilic CdTe-MPA QDs and hydrophilic SPIONs ($n = 6$) was determined after appropriate dilutions (10 times) with double distilled water using Delsa™ Nano C Particle Analyser (Beckman Coulter, USA).

2.2.3. Zeta potential measurement

The stability of the hydrophilic CdTe-MPA QDs and hydrophilic SPIONs (n = 6) was determined by zeta potential after appropriate dilutions (10 times) with Milli-Q water using Delsa™ Nano C Particle Analyser (Beckman Coulter, USA).

2.2.4. Transmission electron microscopy (TEM)

For determining the morphology and size of the prepared hydrophilic CdTe-MPA QDs and hydrophobic and hydrophilic SPIONs, TEM was carried out using JEOL, JEM-2100 electron microscope with an acceleration voltage of 200 kV at various magnifications. To deposit the SPIONs onto the carbon-coated copper grids, these grids were dipped in the prepared aqueous dispersion of CdTe-MPA and SPIONs and dried at room temperature for TEM sample preparation. An average of 10–20 field views of QDs were considered for recording the observations(El-Nahass et al., 2014).

2.2.5. Powder X-ray diffraction (PXRD)

The crystalline or amorphous nature of hydrophilic CdTe-MPA QDs and hydrophilic SPIONs was confirmed by X-ray diffraction measurements carried out with the help of an X-ray diffractometer (PANanalytical, Almedo, Netherlands). PXRD studies were performed by exposing the lyophilized sample (0.15–0.2 g) to CuK_α radiation (45 kV, 40 mA) and scanning from 5° to 50°, 2Θ at a step size of 0.017° and scan step time of 25 s. The instrument measures interlayer spacing 'd' which is calculated from the scattering angle Θ using Bragg's equation $n\lambda = 2d \sin\Theta$, where λ is the wavelength of the incident X-ray beam and n is the order of the interference. The overlaid diffractograms were prepared using Origin Pro 8 software(Yi and Wei, 2017).

2.2.6. Superconducting quantum interference device (SQUID) study

To determine the magnetic properties of the prepared SPIONs, SQUID analysis was carried out using a SQUID magnetometer (Quantum Design MPMS-XL) (Škrátek et al., 2020). This was done by depositing the powder sample packed in non-magnetic teflon tape onto a plastic tube designed especially for the most effective and sensitive measurement. The sample was examined at room temperature with field strength of 2 Tesla.

2.2.7. Absorption and fluorescence spectroscopy

Absorption spectra (λ_{max}) of the synthesized hydrophilic CdTe-MPA QDs was determined from 200 nm to 400 nm using UV–Vis spectrophotometer (PerkinElmer UV/Vis Spectrometer Lambda 35) and photoluminescence (PL) spectra were recorded with an excitation wavelength of 400 nm using Hitachi F-2500 Fluorescence Spectrophotometer(Tirado-Guizar et al., 2015).

2.2.8. Effect of concentration on the emission intensity of CdTe-MPA QDs

The effect of CdTe-MPA QDs concentration on the emission intensity was investigated by PL spectroscopy. Different concentrations of CdTe-MPA QDs were taken and the standard plot was made by plotting these concentrations against the PL intensity.

2.2.9. Measurement of quantum yield

The quantum yields of the free hydrophilic CdTe-MPA QDs, and aptamer conjugated CdTe-MPA QDs were calculated using a Hitachi F-2500 fluorescence spectrometer as per the published procedure using Rhodamine 6G dissolved in absolute ethanol as the reference standard (quantum yield 100%, concentration 31 nmoles/mL). The relative quantum yield of the QDs was calculated from the Eq. (1) given below(Yu et al., 2003).

$$QYNC = QY\ Dye\ mNC/mDye\ x\ (\eta Solvent/\eta Ethanol)^2 \quad (1)$$

Where water was used as a solvent, QY Dye is the quantum yield (QY) of Rhodamine 6G (100%) and ηethanol, and ηsolvent are the refractive indices of the solvents in which the dye and the nanocrystal (NC) sample were dissolved, m is the slope from the plot of the integrated fluorescence intensity versus the absorbance of the sample.

2.3. Selective capturing and bacterial detection using aptamers

Both (CA)-SPIONs and CdTe-MPA QDs (1 mL each, 167 nmoles/ mL) were activated separately by adding 25 μL 1-ethyl-3-(3-dimethylaminopropyl) carbodiimide hydrochloride (EDC; 400 mM in methanol) and 25 μL N-hydroxysuccinimide (NHS; 100 mM in methanol) with constant stirring at room temperature for 30 min. Subsequently, the activated NPs were stored at 4 °C until further use(Singh et al., 2016).

2.3.1. Bioconjugation of NPs with aptamer

Activated SPIONs were mixed with 20 μg/mL of aptamer I and activated CdTe-MPA QDs were mixed with aptamer II (20 μg/mL) prepared in tris-EDTA buffer, pH 8 and reacted for 2 h at 8–10 °C. Aptamer I-conjugated SPIONs and aptamer II-conjugated CdTe-MPA QDs were separated as sediments from the excess free aptamer by centrifugation at 5000 rpm for 15 min. This was followed by washing in triplicates to completely remove the free aptamer. The purified aptamer I conjugated SPIONs and aptamer II conjugated CdTe-MPA QDs were stored at 4 °C separately.

2.4. Bacterial detection

A suspension of *E. coli* (containing 100–500 cfu/mL) was taken aseptically in a suitably labelled Eppendorf tube, to which the aptamer I conjugated hydrophilic SPIONs were added. After incubation for 1 h, the SPION nanoparticles were separated in the form of sludge/pellet, using a magnet with strength of 5000 gauss. This was followed by a thorough washing step repeated thrice. The sludge/pellet was separated from the supernatant (with the help of the magnet) after the third washing, and the supernatant was discarded. Subsequently, aptamer II conjugated CdTe-MPA QDs were added to the pellet and incubated for another 20–30 min, followed by washing twice with sterilized Milli-Q (MQ) water. This complex was then subjected to the following tests for the detection of *E. coli*.

2.5. Bacterial detection using fluorescence spectrophotometry

The effect of concentration of aptamer II on the emission intensity of CdTe-MPA QDs was investigated by PL spectroscopy. Different concentrations of aptamer II conjugated CdTe-MPA QDs were taken and a standard plot was generated by plotting these concentrations against PL intensity.

2.6. Fabrication of in-house developed prototype device for the detection of E. coli

An assembly of the prototype was designed and all the components required were placed and attached to the ATmega328P (Arduino Uno) microcontroller for the proper working of the biosensor, as shown in Fig. 1a. ATmega328P microcontroller was connected to a power source of 9 V. A UV LED, photodiode, and LCD were connected to ATmega328P microcontroller. A sample holder was placed in the middle of the UV light source and photodiode, as shown in Fig. 2d. Fig. 2j represents the ports

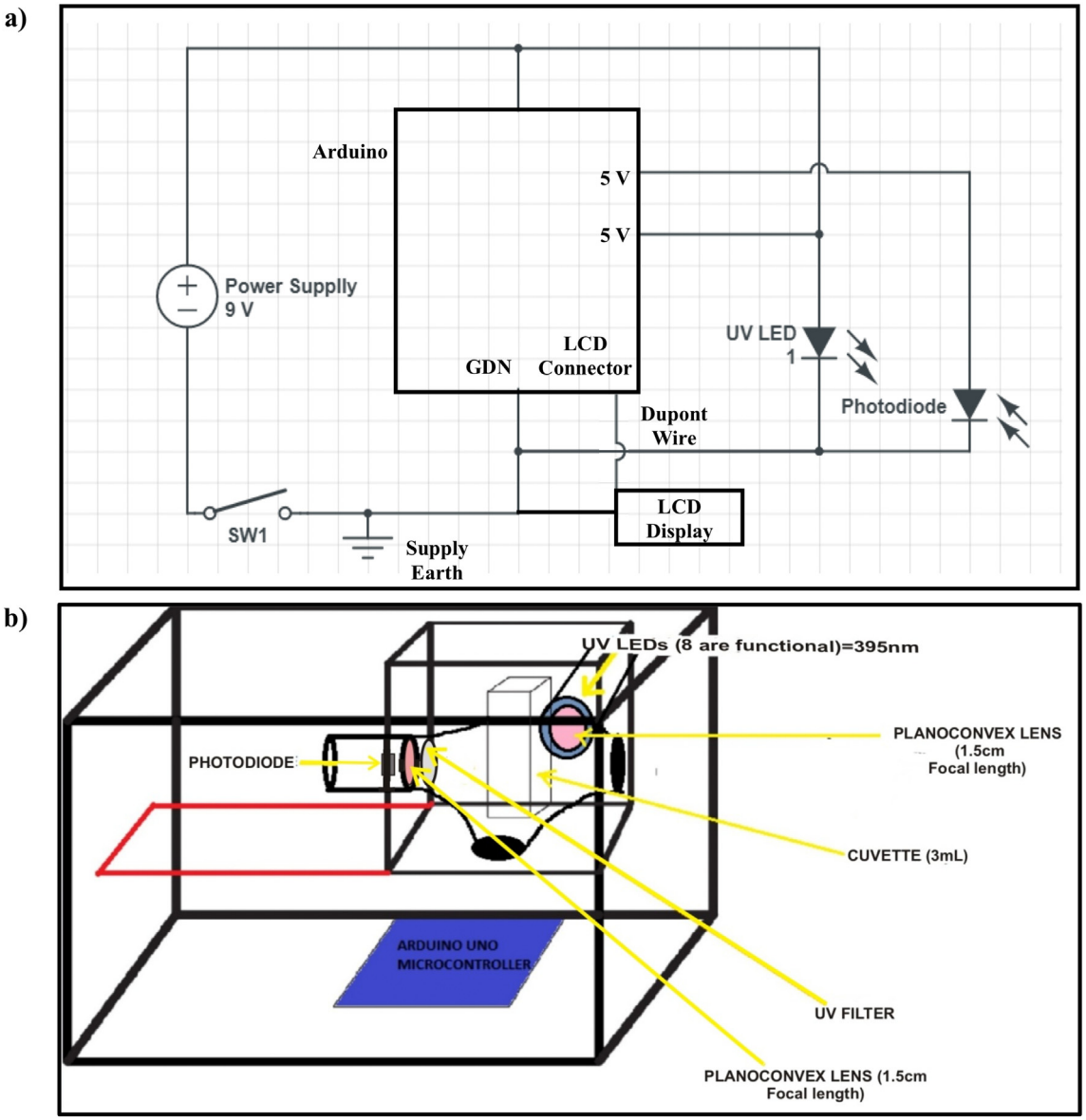

Fig. 1. a) Circuit diagram for Arduino Uno based biosensor b) 3D diagram of Arduino Uno based biosensor.

created for software installation, power source (AC-to-DC adapter or battery), and ON/OFF switch. Moreover, plano-convex lenses were fixed in between the sample holder and the UV light source; and between the sample holder and photodiode, as depicted in Fig. 1b. The life evaluation diagram of the biosensor is given in Fig. 3.

3. Results and discussion

3.1. Synthesis of nanoparticles

The elaborated methodology on synthesis and ligand exchange of SPIONs is given in the SI **Fig. S1 and S2 (Fig. S: Supplementary Figure)**. Detailed methodology on synthesis of CdTe-MPA QDs is given in SI **(Figs. S3 and S4)**.

3.2. Characterization of NPs

3.2.1. Particle size analysis and polydispersity index (PDI)

Dynamic light scattering (DLS) was used to measure the size distribution of the prepared hydrophilic CdTe-MPA QDs and hydrophilic SPIONs dispersed in ultrapure water. The average particle size of hydrophilic CdTe-MPA QDs was found to be 132.9 nm, and for hydrophilic SPIONs, it was 238.9 ± 15.1 nm, as measured by DLS and shown in **Fig. S5** (Hao and Liu, 2016). The PDI of the synthesized hydrophilic CdTe-MPA QDs and hydrophilic SPIONs was 0.243 and 0.309 respectively, as shown in **Fig. S6**. NPs with PDI in the range of 0.1–0.4 are considered to be moderately polydisperse and are approved for use (Bhattacharjee, 2016).

3.2.2. Zeta potential and transmission electron microscopy (TEM)

The Zeta potential of the hydrophilic CdTe-MPA QDs and hydrophilic SPIONs was −13.27 mV and − 8.62 mV, respectively, as shown in **Fig. S7**. Further, the hydrophilic CdTe-MPA QDs and hydrophilic SPIONs were found to be negatively charged, which prevents their excessive aggregation in buffer solution due to the repellent forces among particles. **Fig. S8** depicts TEM images of hydrophilic CdTe-MPA QDs and hydrophilic SPIONs, suggesting the formation/ synthesis of spherical CdTe-MPA QDs with the particle size of about 3 to 5 nm and spherical CA-SPIONs with size in the range of 10.14 to 11.77 nm. All the CdTe QDS and CA-SPIONs had the same shape and appeared to exist singly. DLS studies provide hydrodynamic diameter, thus, justifying a larger particle size obtained in the studies.

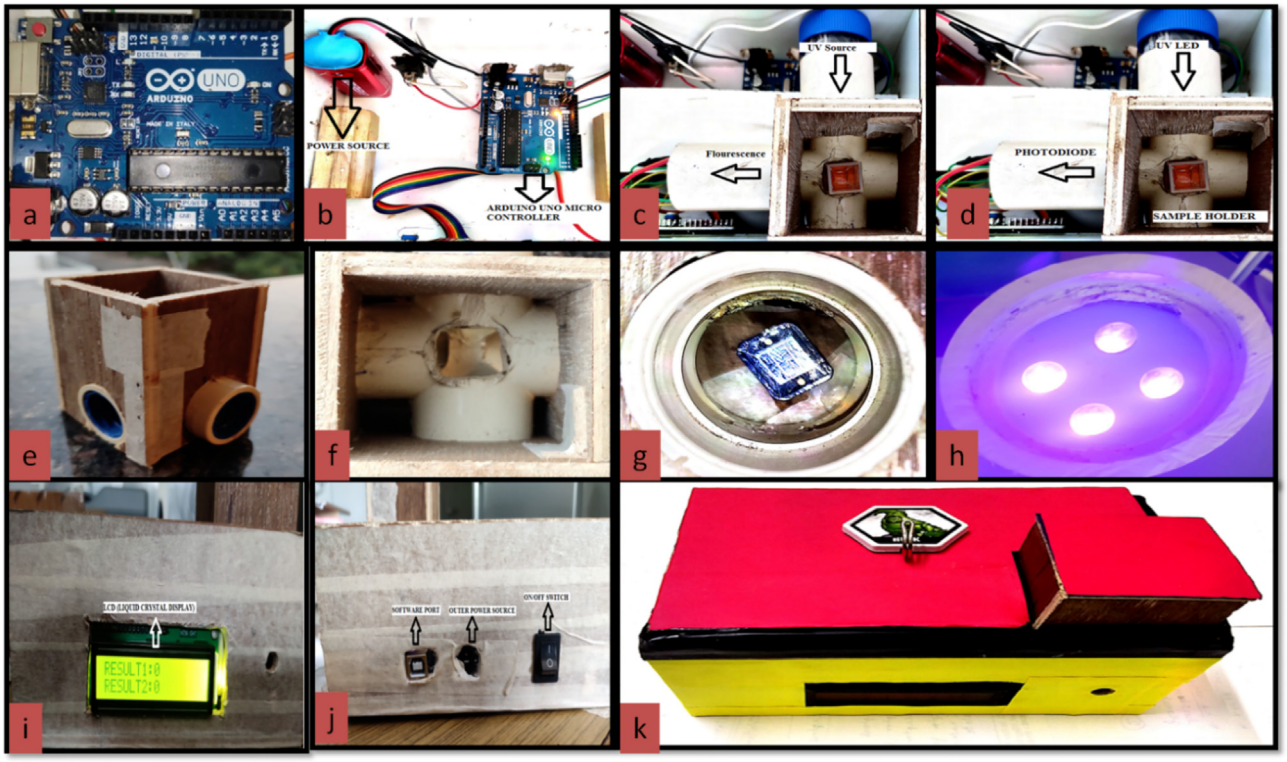

Fig. 2. Schematic representation of fabrication of device a) Arduino Uno microcontroller b) Microcontroller attached with battery source (c), (d) UV source, sample holder, fluorescence detector e), f) Design of sample holder g) Photodiode h) UV LED i) LCD for display of result j) ON/OFF switch, software update port, port for outer power source k) Final prepared prototype biosensor.

3.2.3. Powder X-ray diffraction pattern (PXRD) of CdTe-MPA QDs and SPIONs

PXRD pattern of CdTe-MPA QDs and SPIONs were observed by plotting counts (y-axis) vs. position 2θ (x-axis), as shown in **Fig. S9** (Vo et al., 2016). The PXRD pattern of the CdTe-MPA QDs exhibited peaks at 25°, 43°, and 50° diffractions indicating its crystalline nature, as shown in **Fig. S9a**. PXRD pattern of the SPIONs exhibited peaks at 2θ scattered angles of 30.4243°, 35.8019°, 43.3951°, 53.8799°, 57.4093° and 63.0408°, indicating its crystalline nature (Thuy et al., 2010), as shown in **Fig. S9b.**

3.2.4. Superconducting quantum interference device (SQUID) study of SPIONs

The magnetic property of the SPIONs was examined at room temperature by using a superconducting quantum interference device magnetometer. **Fig. S12** indicates that the SPIONs are superparamagnetic in nature and the net magnetization of the particles in the absence of an external field was zero. Furthermore, no hysteresis was seen when magnetization studies were performed on Fe_3O_4 nanoparticles at room temperature. Under a large external field, the magnetization of the particles aligned within the

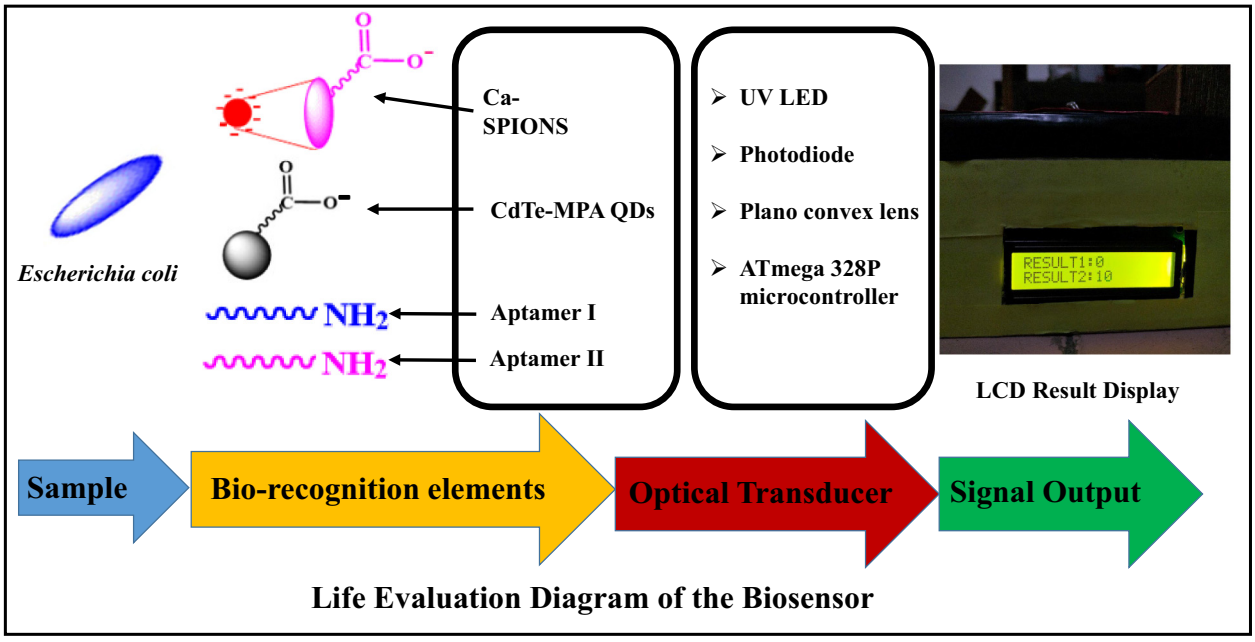

Fig. 3. The figure depicts life evaluation diagram of the biosensor.

field direction and reached its saturation value (saturation magnetization, σs). Further, no coercivity or magnetic remanence was observed, which is typical of superparamagnetic NPs (Kumar et al., 2012).

3.2.5. Absorption spectroscopy and fluorescence spectroscopy of CdTe-MPA QDs

CdTe-MPA QDs stabilized with MPA showed an absorption maximum at 224 nm and were observed by UV–Vis spectrophotometer, as shown in **Fig. S13a**. When observed under a spectrofluorometer, the CdTe-MPA QDs showed a prominent emission peak at 667 nm when excited at 390 nm, as illustrated in **Fig. S13b**. This was consistent with the quantum confinement effects and was in agreement with the slight orange-red color obtained. It was observed that the emission spectrum of QDs exhibited good symmetry with a narrow spectral width. This facilitates an adequate spectral resolution for quantitative detection of the fluorescence intensity. Thus, the results indicate that CdTe-MPA QDs have sharp fluorescence intensity and can be explored as a potential fluorescent probe for detection (Torchynska and Vorobiev, 2011).

3.2.6. Effect of concentration on the emission intensity of CdTe-MPA QDs

The effect of concentration on fluorescence intensity of CdTe QDs was found to be increasing i.e., from 10 μg to 100 μg when validated for 5 days. **Fig. S14 (a-e)** shows a prominent emission peak for hydrophilic CdTe-MPA QDs at 637 nm when excited at 390–400 nm. On gradually increasing the concentration of QDs, an increase in emission intensity was observed which establishes the fact that the emission intensity is directly proportional to the concentration of the CdTe-MPA QDs. A slight shift in emission wavelength was observed, which might be due to the different excitation wavelengths (390–400 nm). The test for fluorescence stability of water dispersible CdTe-MPA was conducted at different concentrations from 10 μg to 100 μg at pH 7.0 and analyzed using a spectrofluorometer independently for 5 consecutive days.

3.2.7. Measurement of quantum yield

Mean photoluminescence quantum yields of the CdTe-MPA QDs and conjugated QDs, measured using Rhodamine 6G as a reference standard, were found to be 38 ± 2% and 21 ± 5%, respectively. Thus, it is quite evident from the results that the quantum yield of conjugated QDs relative to that of non-conjugated ones was about 79%. Since quantum yield is a measure of the optical quality of fluorophores, the resultant high value of quantum yield suggest substantial retention of fluorescent properties of QDs even after conjugation(Ferrari and Bergquist, 2007; Yu et al., 2003).

3.3. Selective capturing and bacterial detection using aptamers

To successfully detect the pathogen, the aptamers hand-picked against *E. coli* had to be conjugated with their respective nanoparticles (both SPIONs as well as CdTe-MPA QDs) to result in an efficient system. In order to achieve this, both types of nanoparticles were subjected to EDC/NHS activation, which resulted in the formation of highly reactive intermediates (NHS-carboxylate)(Tripathi et al., 2016). EDC, a zero-length cross-linker, was selected for bioconjugation, since it is the most commonly used coupling agent. Moreover, it is known to produce higher yields of bioconjugates in a controlled manner with high efficiencies. This intermediate was further used to attach the aptamer.

3.3.1. Bioconjugation of CA-SPIONs and CdTe-MPA QDs with aptamer I and II

After the activation with EDC/NHS, the addition of aptamer I and II to the reactive intermediate resulted in the formation of amide linkage between the amino group of the DNA oligonucleotide and NHS ester. This led to the formation of the desired nanoconjugates of aptamer I-CA-SPIONs and aptamer II-CdTe-MPA QDs.

3.3.2. Confirmation of bioconjugation of CA-SPIONs and CdTe-MPA QDs with aptamer I and II

This was done to confirm whether the water-dispersible nanoparticles have indeed been conjugated with the respective aptamers and also to validate/confirm the fluorescent nature of CdTe-MPA QDs after bioconjugation with the aptamer.

3.3.2.1. FTIR of SPIONs and CdTe-MPA QDs. FTIR spectra for both the SPIONs (conjugated as well as unconjugated) were recorded to confirm the presence of an amide bond formed due to the amino group of the aptamer I and NHS carboxylate intermediate (conjugated SPIONs) or a coating layer consisting of CA on the surface of the SPIONs, as shown in **Fig. S11a**. To verify whether the respective aptamer has efficiently attached with CA, FTIR spectra of the bioconjugated SPIONs **(Fig. S19a)** were also recorded. The spectrum showed characteristic peaks at 1663 cm^{-1} and 1613 cm^{-1} which are typical of the carbonyl groups for amide linkages, and at 3425 cm^{-1}, which is probably due to the -NH group of the amide bond. It also showed a significantly enhanced -CH_2 peak (in context to those observed in **Fig. S11a** for CA-SPIONs) observed at 2923 cm^{-1}, which confirms bioconjugation(Lattuada and Hatton, 2007). **Fig. S20a** depicts that the aptamer II has been efficiently attached. The spectrum showed characteristic peaks at 1660 cm^{-1} which is typical of the carbonyl groups for amide linkages and a sharper peak was recorded at 3426 cm^{-1}, which is probably due to the -NH group of the amide bond in contrast to the broader peak of –OH group observed for unconjugated CdTe-MPA QDs, as shown in **Fig. S20b**. It also shows a significantly enhanced -CH_2 peak observed at 2935 cm^{-1}, which further confirms bioconjugation (Lattuada and Hatton, 2007).

3.3.2.2. Fluorescence properties of CdTe-MPA QDs. When observed under a spectrofluorometer, the CdTe-MPA QDs showed prominent emission peak at 667 nm when excited at 390 nm, as illustrated in **Fig. S13b.** Fig. 4a depicts the emission spectra of non-conjugated CdTe-MPA QDs with a prominent emission peak at 667 nm on excitation at 390 nm. Moreover, a minuscule bathochromic shift (i.e., peak position shift towards longer wavelength) was also observed for the conjugated CdTe-MPA QDs. Nevertheless, two-fold reduction in emission spectra was observed with aptamer II-conjugated CdTe-MPA QDs. This decrease in the fluorescence intensity of CdTe-MPA QDs on bioconjugation with aptamer II is attributed to changes in the electronic energy caused by interactions which occurred on the surface of CdTe-MPA QDs during the bioconjugation process. It may however, be noted that the quantum yield of the aptamer II conjugated CdTe-MPA QDs (Section 2.2.7) was still 79% and the fluorescence was experimentally significant.

3.4. Bacterial detection

3.4.1. Bioconjugated CA-SPIONs and CdTe-MPA QDs for bacterial detection

A concentration of 10 μM of *E. coli* specific aptamer I & II conjugated to the CA-SPIONs (Fig. 5a**)** and CdTe-MPA QDs (1 mL each) **(**Fig. 5b**)** containing 2 μg/L of CA-SPIONs and 167 nM of CdTe-MPA QDs respectively were selected for the detection of *E. coli.* Water samples containing *E. coli* cells were incubated with *E. coli* specific aptamer I conjugated CA-SPIONs. These immediately get attached to *E. coli* cells due to the presence of the highly specific aptamer I on the surface of SPIONs. Afterward, they were separated using a high strength laboratory magnet to form a sludge consisting of the bacteria-SPION complex. The presence of the trapped *E. coli* cells can be verified with the help of aptamer II–conjugated CdTe-MPA QDs. Once appropriate washings have been done (to remove the supernatant), the addition of aptamer II conjugated CdTe-MPA QDs yielded positive results when viewed with the help of different techniques. These studies affirm the utility of both types of NPs, viz. CA-SPIONs and CdTe-MPA QDs, each conjugated with an *E. coli* specific aptamer capable of detecting even a low count of 100 *E. coli* cfu. Fig. 6 shows CLSM, Field Emission Scanning Electron Microscope (FESEM) and Gram staining results of *E. coli*-aptamer II-conjugated CdTe-MPA QDs. This confirms the attachment of conjugated nanoparticles onto the *E. coli* cells.

3.4.2. Bacterial detection using fluorescence spectrophotometry

Fluorescence spectra of bacteria captured with Aptamer II conjugated CdTe-MPA QDs was observed under a spectrofluorometer, the Aptamer II

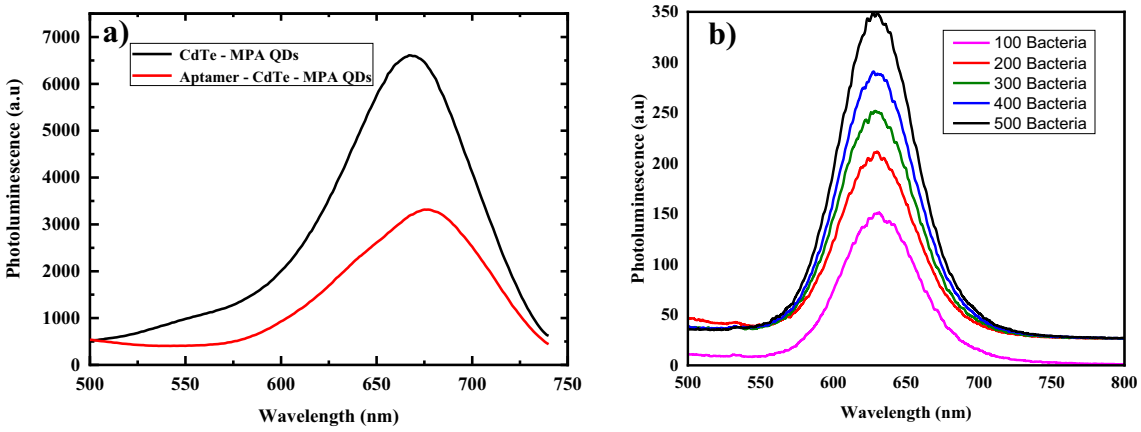

Fig. 4. a) Fluorescence intensity of unconjugated CdTe-MPA QDs, and aptamer conjugated CdTe-MPA QDs b) Fluorescence spectra of *E.coli* captured-aptamer conjugated CdTe-MPA QDs (1 mg/mL).

conjugated CdTe-MPA QDs showed a prominent emission peak at 667 nm when excited at 390 nm, as illustrated in Fig. 4a. Fig. 4b shows a prominent emission peak of *E. coli*-Aptamer II-conjugated CdTe-MPA QDs (pH 7) at 667 nm when excited at 390–400 nm. On gradually increasing the concentration of *E. coli* cfu, an increase in emission intensity was observed which establishes the fact that the emission intensity is directly proportional to the concentration of the CdTe-MPA QDs attached onto the surface of *E. coli* cells. A slight shift in emission wavelength was observed, which might be due to the different excitation wavelength (390–400 nm). **Fig. S25 (a-c)** shows prominent emission peaks of *E.coli*-Aptamer II-conjugated CdTe-MPA QDs at pH 6.0, 8.0 and 9.0. On gradually increasing the number of *E. coli* cells, an increase in emission intensity was observed, which establishes the fact that varying the pH has no significant effect on the sensitivity of detection.

3.5. Fabrication of in-house developed prototype biosensor for the detection of E.coli

ATmega 328P microcontroller was selected for the development of a prototype biosensor as shown in Fig. 2. In brief, the light from the UV LED uniformly illuminates the sample contained in the cuvette, while the photodiode detects the fluorescent emission. Additionally, plano-convex lenses were used to focus light emitted from the sample holder onto the photodiode; wherein, these lenses increase the light arriving on the photodiode so that light sources with lower light intensity can be used(Dutta, 2019). ATmega 328P microcontroller was connected to a photodiode for sensing emission from water samples containing the Aptamer II conjugated CdTe- MPA QDs attached to *E. coli* cells. Further, the photodiode converts light into the electrical current; the generated current is displayed on LCD in the form of numerical values. The circuit diagram for the prototype biosensor is shown in Fig. 1a.

3.5.1. Fluorescence measurement of CdTe-MPA QDs by prototype biosensor

Fluorescence intensity readings of CdTe-MPA QDs were monitored on the LCD of the prototype biosensor (before and after excitation by UV light, as shown in Fig. 7a and b. The values of the fluorescence intensity were recorded for the QDs up to a least limit of 100 μg/mL and the highest limit of 400 μg/mL. The results were optimized for three consecutive days, further; it was observed that the UV light was causing interference with the signals below 100 μg/mL, due to which the prototype biosensor was unable to produce a signal for low count. Thus, the sensitivity limit of the prototype biosensor was observed to be 100 μg/mL - 400 μg/mL. The results recorded as digital signals on LCD were calculated by conversion of millivolts (mV), since, in ATmega 328P microcontroller, 5 V is equal to 1024 (Arduino, 2020). The LCD screen of biosensor exhibits Result 1 and Result 2. Result 1, which was not connected to photodiode, consequently not considered for the detection of fluorescence. Whereas, Result 2 (Fig. 7c) shown in the LCD was the desired result, as it exhibited maximum fluorescence produced by QDs when excited by wavelength of 400 nm and hence, confirmed that the biosensor prototype was functioning well. Fig. 7 **(c-e)** depicts the correlation between the current generated due to the increased fluorescence intensity. As, with 100 μg/mL, the digital signal was found to be 10 (48.83 mV), for 200 μg/mL, the digital signal was found to be 13 (63.48 mV) and for 400 μg/mL, the digital signal was found to be 17 (83 mV). Thus, all these results depicted that CdTe-MPA QDs were able to produce sufficient and concentration dependent fluorescence intensity, thereby confirming the immense potential of a prototype biosensor for pathogen detection.

3.5.2. Fluorescence measurement of E. coli captured Aptamer II-conjugated CdTe-MPA QDs by prototype biosensor

Fluorescence intensity readings of *E. coli* captured aptamer II conjugated CdTe MPA QDs were monitored on the LCD of the prototype biosensor.

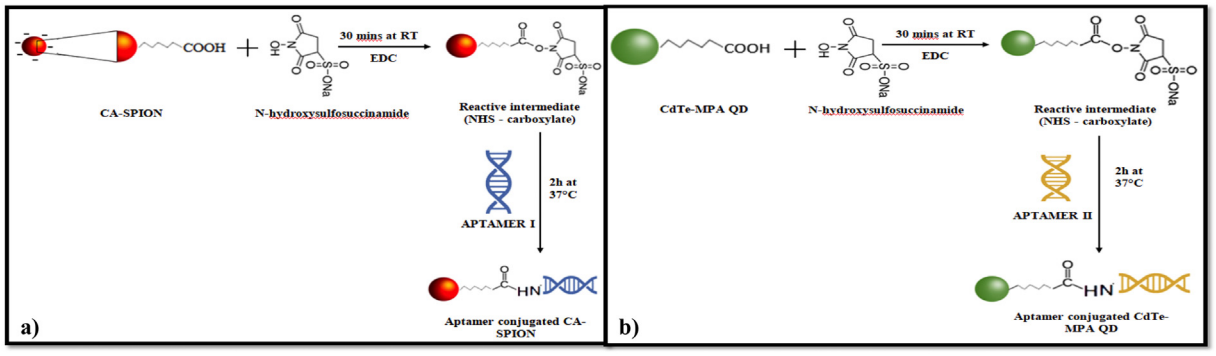

Fig. 5. a) Diagrammatic representation of the preparation of aptamer conjugated CA-SPIONs b) Diagrammatic representation of the preparation of aptamer conjugated CdTe-MPA QDs.

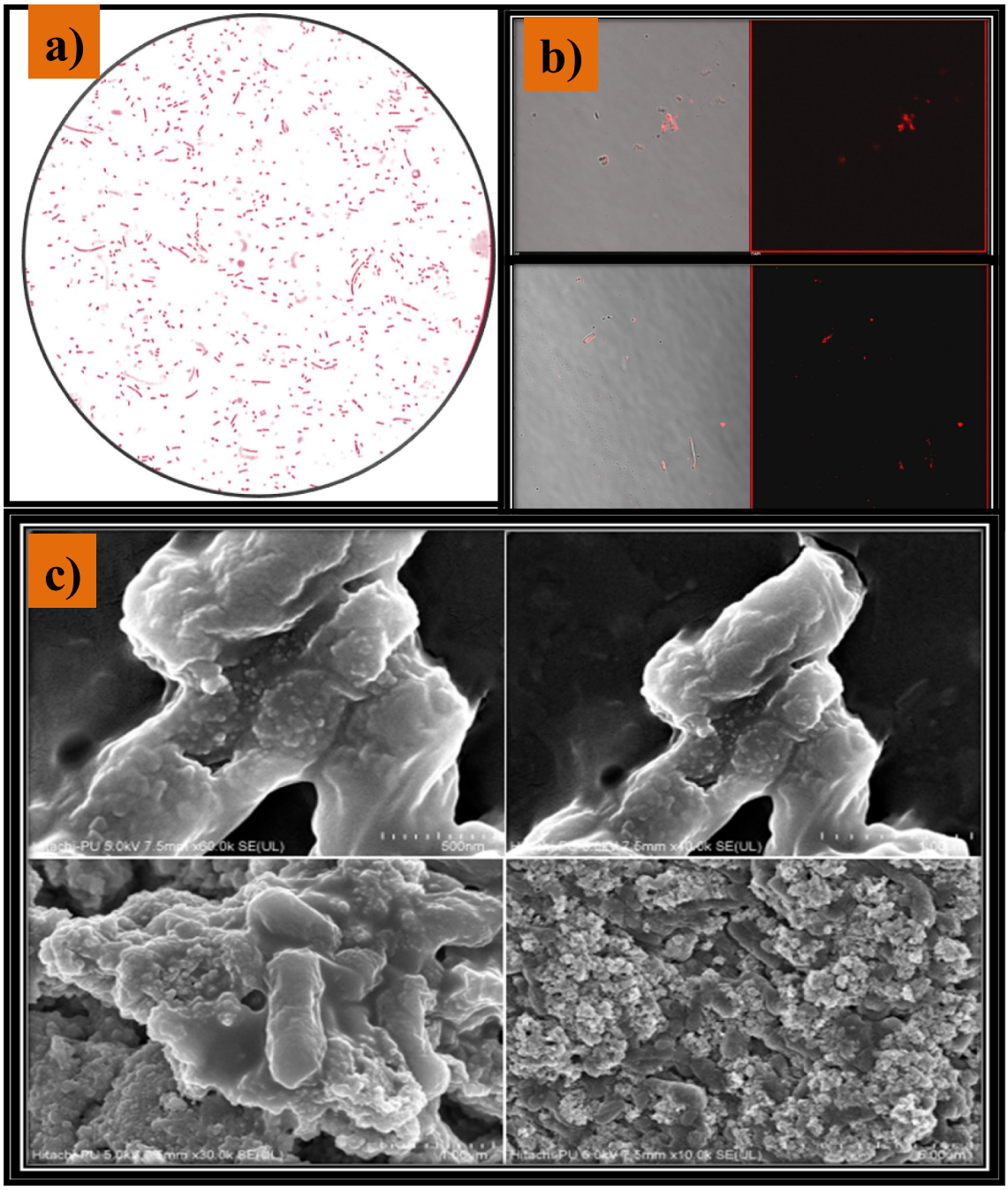

Fig. 6. Depiction of a) Gram staining, b) CLSM and c) FESEM results for *E. coli* aptamer II conjuagted CdTe MPA QDs.

Result 2 shown in the LCD was considered for the detection of fluorescence, as mentioned above. The fluorescence intensity values were recorded for 100, 200, 300, 400 and 500 cfu, each having100 μg/mL CdTe-MPA QDs. The results were optimized for three consecutive days and it was observed that for 100 cfu, the prototype biosensor was able to produce a digital signal of 6 (29.3 mV) **(**Fig. 8a**)**, for 200 cfu the digital signal was found to be 7 (34.18 mV) **(**Fig. 8b**),** for 300 cfu the digital signal was found to be 8 (39.06 mV) **(**Fig. 8c**)**, for 400 cfu the digital signal was found to be 9 (43.94 mV) **(**Fig. 8d**)** and for 500 cfu, the digital signal was found to be 10 (48.82 mV) **(**Fig. 8e**)**. Thus, all these results depict that aptamer II conjugated CdTe-MPA QDs were selectively able to capture *E. coli* and produced sufficient fluorescence signals. Eventually, the prototype biosensor justifies the utility of aptamer II conjugated CdTe-MPA QDs for the detection of even a low count of 100 *E. coli* cells. Further studies are needed to validate and quantify the experimental results.

3.6. Signal reproducibility study of biosensor for bacterial concentration at different pH

The *E. coli* samples were subjected to different pH i.e., 6, 8 and 9 and were tested with our biosensor device at different time intervals (at 5 min interval upto 25 min). Further, it confirms that the digital signals exhibited by biosensor at aforementioned pH are reproducible. The photographic images of digital signals are shown in **Figs. S26–28**.

4. Conclusions

The current research work reports the successful development of a fluorescence-based ATmega328P prototype biosensor for the efficient detection of *E. coli*. SPIONs and CdTe-MPA QDs were synthesized using thermal decomposition method and direct aqueous method respectively, and

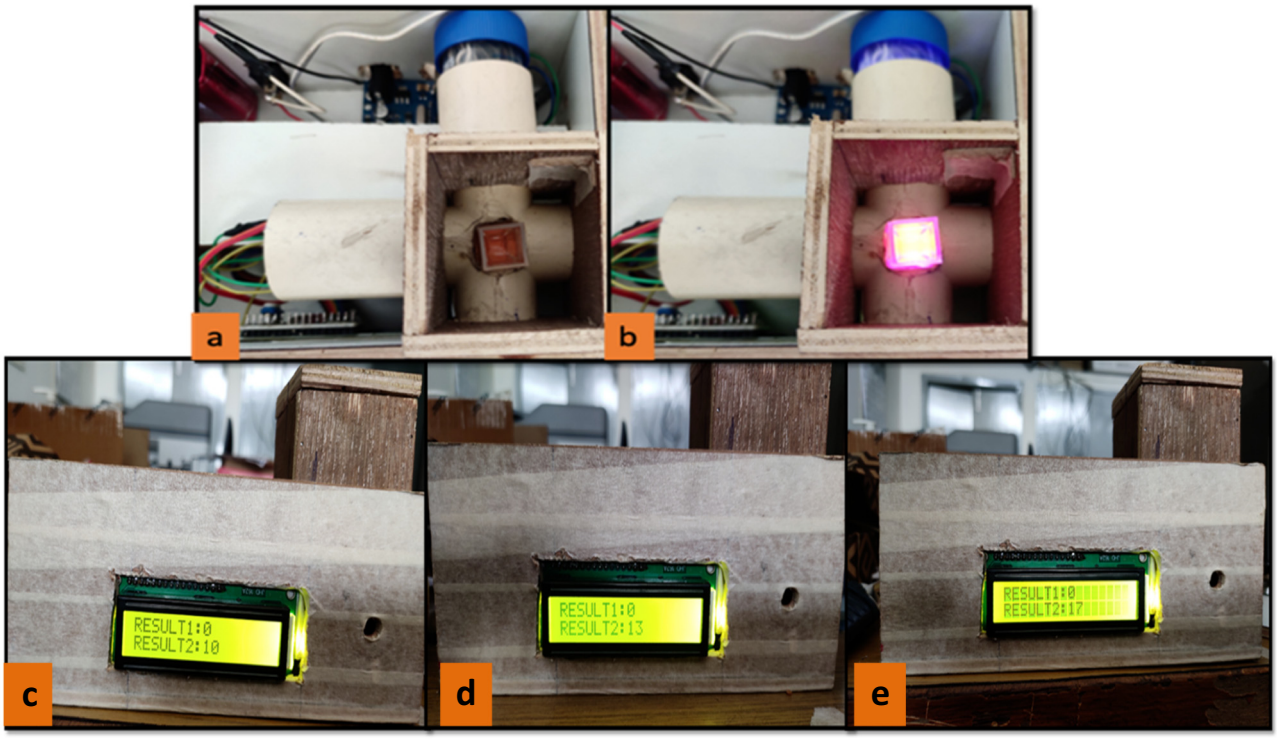

Fig. 7. Photographic image of device of the upper panel shows a) before excitation by UV light and b)after excitation by UV light: Photographic image of device in the below panel showing result for c) 100 μL of CdTe-MPA QDs in 900 μl Milli-Q water (1:10) d) 200 μL of CdTe-MPA QDs in 800 μL Milli-Q water (1:4) and e) 400 μL of CdTe-MPA QDs in 600 μL Milli-Q water (1:1.5).

were confirmed to be monodispersed and spherical shaped. Both types of nanoparticles were then conjugated with *E. coli* specific aptamer I & II. SQUID and high quantum yield with significant magnetic and fluorescent characteristics justify the utility of conjugated SPIONs and CdTe-MPA QDs as an effective microbial detection tool. Bioconjugation of *E. coli* specific aptamer I &II with SPIONs as well as QDs studied using various

Fig. 8. Photographic image of the device showing result for a) 100 μl of CdTe-MPA QDs with 100 cfu b) 100 μl of CdTe-MPA QDs with 200 cfu c) 100 μl of CdTe MPA QDs with 300 cfu d) 100 μl of CdTe-MPA QDs with 400 cfu and e) 100 μl of CdTe-MPA QDs with 500 cfu.

methods demonstrated selective separation and subsequently, detection of *E. coli*. Aptamer II conjugated CdTe MPA QDs were further used for the capture and detection of *E.coli* with the ATmega 328P prototype biosensor. The biosensor can detect up to100 cfu in the sample, which reflects the sensitivity of the developed technique. It offers on-spot detection, ease of usage and is less time consuming. In a nutshell, ATmega328P prototype biosensor and cadmium-based QDs hold immense potential for the efficient detection of *E. coli* in water samples. The technology can be rationally extended and explored for the detection of other pathogenic microorganisms in a myriad of food samples. Further, the system fulfills the need to develop a miniaturized and portable field deployable device for pathogen detection.

CRediT authorship contribution statement

Conceptualization: Gurpal Singh (GS), Ravi Pratap Barnwal (RPB), Indu Pal Kaur (IPK), Udit Soni (US), Sameer Sapra (SS) were involved in the conceptualization of manuscript.

Data curation; Natarajan Gopalan (NG), Bhupinder Singh(BS), GS, RPB, Chitvan Pandit (CP), Joga Singh (JS), Hema Kumari Alajangi (HKA), Akhil Khajuria (AK), Akanksha Sharma (AS) were involved in task of data curation.

Formal analysis; GS, RPB, IPK, CP, JS, HKA, AK and AS were involved in formal analysis of the manuscript.

Funding acquisition; Anil Dutt Semwal (ADS), Manmohan Parida (MP) and Rakesh Kumar Sharma (RKS) were responsible for funding acquisition.

Investigation; CP, JS, AK, IPK, RPB and GS were involved the investigation for all the experimental work related to the project.

Methodology; GS, RPB, HKA, JS, CP, AK, were involved in preparation of methodology for the conduct of experiments.

Project administration; GS, RPB, NG, BS, US, Ashish Suttee (AS) and IPK were involved in the job of project administration.

Resources; GS, RPB, IPK, JS, RKS, NG and ADS were involved in collecting resources necessary for successful completion of the project.

Software; Md.Samim Hassan (MSH), AS, AK, HKA and RPB were involved in software handling for the manuscript.

Supervision: GS, RPB, IPK, US, SS and RKS were involved in supervision of the project and successful writing of manuscript.

Validation; BS, IPK, GS, RPB, NG and RKS were involved in the validation of all the experimentations for the project.

Visualization; BS, IPK, GS, RPB, NG, AS and RKS were involved in visualization of the manuscript to form a precise.

Roles/Writing – original draft; AK, JS, HKA, AS, GS and RPB prepared the original manuscript. RPB, HKA and AS prepared the diagrammatic representations for the manuscript.

Writing – review & editing. GS, RPB and IPK carried out the reviewing and editing of the manuscript.

Declaration of competing interest

The authors declare that they have no known competing financial interests or personal relationships that could have appeared to influence the work reported in this paper.

Acknowledgements

The authors gratefully acknowledge the financial grants received from DFRL (DRDO) (Sanction letter no. 1634/P&C dt.14.03.2018), Government of India. RPB and GS appreciate the support granted by UGC, New Delhi, India, under Faculty Recharge Program. RPB and GS gratefully acknowledge the financial grant received from DBT (BT/PR27444/BRB/10/1645/2018) and ICMR (35/2/2020-Nano/BMS), Government of India. HKA acknowledges DHR, Government of India (YSS/2020/000047/PRCYSS) for the financial support.

Appendix A. Supplementary data

Supplementary data to this article can be found online at https://doi.org/10.1016/j.scitotenv.2022.154857.

References

Alahi, M.E.E., Mukhopadhyay, S.C., 2017. Detection methodologies for pathogen and toxins: a review. Sensors (Switzerland) https://doi.org/10.3390/s17081885.
Arduino, 2020. URL https://www.arduino.cc/reference/en/language/functions/analog-io/analogread/ (accessed 3.11.22).
Bhattacharjee, S., 2016. DLS and zeta potential - what they are and what they are not? J. Control. Release https://doi.org/10.1016/j.jconrel.2016.06.017.
Borah, M., Dutta, J., Misra, A.K., 2010. The bacteriological quality of drinking water in Golaghat Sub-division of Golaghat District, Assam, India. Int. J. ChemTech Res. 2 (3), 1843–1851.
Cabral, J.P.S., 2010. Water microbiology. Bacterial pathogens and water. Int. J. Environ. Res. Public Health https://doi.org/10.3390/ijerph7103657.
Chandran, A., Mazumder, A., 2016. Erratum: Chandran and Mazumder, Pathogenic Potential, Genetic Diversity, and Population Structure of Escherichia coli Strains Isolated from a Forest-Dominated Watershed (Comox Lake) in British Columbia, Canada [Appl Environ Microbiol. Volume 81, no. 5, p. Appl. Environ. Microbiol. https://doi.org/10.1128/AEM.03528-15.
Cho, S., Hiott, L.M., Barrett, J.B., McMillan, E.A., House, S.L., Humayoun, S.B., Adams, E.S., Jackson, C.R., Frye, J.G., 2018. Prevalence and characterization of Escherichia coli isolated from the upper oconee watershed in Northeast Georgia. PLoS ONE https://doi.org/10.1371/journal.pone.0197005.
Dutta, S., 2019. Point of care sensing and biosensing using ambient light sensor of smartphone: critical review. TrAC - Trends Anal. Chem. https://doi.org/10.1016/j.trac.2018.11.014.
El-Nahass, M.M., Youssef, G.M., Noby, S.Z., 2014. Structural and optical characterization of CdTe quantum dots thin films. J. Alloys Compd. https://doi.org/10.1016/j.jallcom.2014.03.104.
Ferrari, B.C., Bergquist, P.L., 2007. Quantum dots as alternatives to organic fluorophores for cryptosporidium detection using conventional flow cytometry and specific monoclonal antibodies: lessons learned. Cytometry A https://doi.org/10.1002/cyto.a.20381.
Gall, A.M., Mari, B.J., Lu, Y., Shisler, J.L., 2015. Waterborne Viruses : A Barrier to Safe Drinking Water, pp. 1–7 https://doi.org/10.1371/journal.ppat.1004867.
Hao, M., Liu, R., 2016. Influence of mercaptopropionic-acid-capped CdTe quantum dots on the human chorionic gonadotropin structure and activity alterations. RSC Adv. https://doi.org/10.1039/c6ra12199c.
Hesari, N., Alum, A., Elzein, M., Abbaszadegan, M., 2016. A biosensor platform for rapid detection of E. coli in drinking water. Enzym. Microb. Technol. 83, 22–28. https://doi.org/10.1016/j.enzmictec.2015.11.007.
Investigating Outbreaks | Foodborne Outbreaks | Food Safety | CDC [WWW Document], n.d. URL https://www.cdc.gov/foodsafety/outbreaks/investigating-outbreaks/index.html (accessed 9.20.21).
Jana, N.R., Chen, Y., Peng, X., 2004. Size- and shape-controlled magnetic (Cr, Mn, Fe, Co, Ni) oxide nanocrystals via a simple and general approach. Chem. Mater. https://doi.org/10.1021/cm049221k.
Jang, J., Hur, H.G., Sadowsky, M.J., Byappanahalli, M.N., Yan, T., Ishii, S., 2017. Environmental Escherichia coli: ecology and public health implications—a review. J. Appl. Microbiol. https://doi.org/10.1111/jam.13468.
Jung, J.K., Alam, K.K., Verosloff, M.S., Capdevila, D.A., Desmau, M., Clauer, P.R., Lee, J.W., Nguyen, P.Q., Pastén, P.A., Matiasek, S.J., Gaillard, J.F., Giedroc, D.P., Collins, J.J., Lucks, J.B., 2020. Cell-free biosensors for rapid detection of water contaminants. Nat. Biotechnol. https://doi.org/10.1038/s41587-020-0571-7.
Kumar, M., Singh, G., Arora, V., Mewar, S., Sharma, U., Jagannathan, N.R., Sapra, S., Dinda, A.K., Kharbanda, S., Singh, H., 2012. Cellular interaction of folic acid conjugated superparamagnetic iron oxide nanoparticles and its use as contrast agent for targeted magnetic imaging of tumor cells. Int. J. Nanomedicine https://doi.org/10.2147/IJN.S32694.
Lattuada, M., Hatton, T.A., 2007. Functionalization of monodisperse magnetic nanoparticles. Langmuir https://doi.org/10.1021/la062092x.
Liu, L., Johnson, H.L., Cousens, S., Perin, J., Scott, S., Lawn, J.E., Rudan, I., Campbell, H., Cibulskis, R., Li, M., Mathers, C., Black, R.E., 2012. Global, regional, and national causes of child mortality: an updated systematic analysis for 2010 with time trends since 2000. Lancet https://doi.org/10.1016/S0140-6736(12)60560-1.
Lukjancenko, O., Wassenaar, T.M., Ussery, D.W., 2010. Comparison of 61 sequenced Escherichia coli genomes. Microb. Ecol. 60, 708–720. https://doi.org/10.1007/s00248-010-9717-3.
Mittal, M., Sapra, S., 2015. Narrowing the size distribution of CdTe nanocrystals using digestive ripening. Pramana - J. Phys. 84, 1049–1054. https://doi.org/10.1007/s12043-015-1007-7.
Singh, G., Kumar, M., Soni, U., Arora, V., Bansal, V., Gupta, D., Bhat, M., Dinda, A.K., Sapra, S., Singh, H., 2016. Cancer cell targeting using folic acid/anti-HER2 antibody conjugated fluorescent CdSe/CdS/ZnS-mercaptopropionic acid and CdTe-mercaptosuccinic acid quantum dots. J. Nanosci. Nanotechnol. 16, 130–143. https://doi.org/10.1166/jnn.2016.10825.
Sivasakthivel, S., Nandini, N., 2014. Health risk assessment of microbial water quality and bioaerosols emission from Byramangala Reservoir, Karnataka, India. Int. J. Sci. Res. 3 (7), 510–514.
Škrátek, M., Dvurečenskij, A., Kluknavský, M., Barta, A., Balíš, P., Mičurová, A., Cigáň, A., Eckstein-Andicsová, A., Maňka, J., Bernátová, I., 2020. Sensitive SQUID bio-

magnetometry for determination and differentiation of biogenic iron and iron oxide nanoparticles in the biological samples. Nanomaterials https://doi.org/10.3390/nano10101993.

Thuy, U.T.D., Toan, P.S., Chi, T.T.K., Khang, D.D., Liem, N.Q., 2010. CdTe quantum dots for an application in the life sciences. Adv. Nat. Sci. Nanosci. Nanotechnol. https://doi.org/10.1088/2043-6262/1/4/045009.

Tirado-Guizar, A., Pina-Luis, G., Paraguay-Delgado, F., 2015. Fluorescence enhancement study of shell-less CdTe quantum dots. Mater. Express 5, 33–40. https://doi.org/10.1166/mex.2015.1211.

Torchynska, T., Vorobiev, Y., 2011. Semiconductor II-VI quantum dots with interface states and their biomedical applications. Advanced Biomedical Engineering https://doi.org/10.5772/20628.

Tripathi, S.K., Khurana, R.K., Kaur, G., Teenu, Singh, B., 2016. Quantum dots: dynamic tools in cancer nanomedicine. Nanobiomaterials in Medical Imaging: Applications of Nanobiomaterials https://doi.org/10.1016/B978-0-323-41736-5.00003-0.

Vo, N.T., Ngo, H.D., Do Thi, N.P., Nguyen Thi, K.P., Duong, A.P., Lam, V., 2016. Stability investigation of ligand-exchanged CdSe/ZnS-Y (Y =3-mercaptopropionic acid or mercaptosuccinic acid) through zeta potential measurements. J. Nanomater. https://doi.org/10.1155/2016/8564648.

WHO/UNICEF JMP, 2017. Progress on Drinking Water, Sanitation and Hygiene WHO Library Cataloguing-in-Publication Data. World Health Organization.

Yi, K.Y., Wei, C.S., 2017. Electrochemiluminescence of CdTe quantum dots and sensitive detection of hemoglobin. Int. J. Electrochem. Sci. https://doi.org/10.20964/2017.04.100.

Yi, J., Xiao, W., Li, G., Wu, P., He, Yayuan, Chen, C., He, Yafei, Ding, P., Kai, T., 2020. The research of aptamer biosensor technologies for detection of microorganism. Appl. Microbiol. Biotechnol. https://doi.org/10.1007/s00253-020-10940-1.

Yu, W.W., Qu, L., Guo, W., Peng, X., 2003. Experimental determination of the extinction coefficient of CdTe, CdSe, and CdS nanocrystals. Chem. Mater. https://doi.org/10.1021/cm034081k.